Published in final edited form as:
*Neuroimage*. 2010 May 1; 50(4): 1464–1471. doi:10.1016/j.neuroimage.2010.01.050.

# Ultrasonic disruption of the blood-brain barrier enables in vivo functional mapping of the mouse barrel field cortex with manganese-enhanced MRI

**Gabriel P. Howles**[1,2], **Yi Qi**[2], and **G. Allan Johnson**[2]

[1] Department of Biomedical Engineering, Duke University, Durham, NC

[2] Center for In Vivo Microscopy, Duke University Medical Center, Durham, NC

## Abstract

Though mice are the dominant model system for studying the genetic and molecular underpinnings of neuroscience, functional neuroimaging in mice remains technically challenging. One approach—Activation-Induced Manganese-enhanced MRI (AIM MRI) —has been used successfully to map neuronal activity in rodents. In AIM MRI, manganese$^{2+}$ acts a calcium analog and accumulates in depolarized neurons. Because manganese$^{2+}$ shortens T1, regions of elevated neuronal activity enhance in MRI. However, because manganese does not cross the blood-brain barrier (BBB), the need to osmotically disrupt the BBB has limited the use of AIM MRI, particularly in mice. In this work, the BBB was opened in mice using unfocused, transcranial ultrasound in combination with gas-filled microbubbles. Using this non-invasive technique to open the BBB bilaterally, manganese could be quickly administered to the whole mouse brain. With this approach, AIM MRI was used to map the neuronal response to unilateral mechanical stimulation of the vibrissae in lightly sedated mice. The resultant 3D activation map agreed well with published representations of the vibrissae regions of the barrel field cortex. The anterior portions of the barrel field cortex corresponding to the more rostral vibrissae showed greater activation, consistent with previous literature. Because the ultrasonic opening of the BBB is simple, fast, and non-invasive, this approach is suitable for high-throughput and longitudinal studies in awake mice. This approach enables a new way to map neuronal activity in mice with manganese.

## Introduction

Functional MRI (fMRI) has revolutionized neuroscience by providing a noninvasive method for mapping neuronal activity in living animals and humans. Typically, fMRI relies the Blood Oxygen Level Dependent (BOLD) contrast, which detects small fluctuations in regional brain perfusion as a proxy for local neuronal activity. While fMRI is used routinely in humans, primates, and even rats, fMRI in the mouse remains a largely out of reach. Nevertheless, because the mouse is the dominant model system for studying the genetic and molecular basis of brain development and disease, there is a tremendous need for a non-invasive tool for mapping neuronal activity in the mouse. Despite this need, the

Correspondence: G. Allan Johnson, Center for In Vivo Microscopy, Box 3302 Duke University Medical Center, Durham, NC 27710, 919 684-7758, gjohnson@duke.edu.

implementation of a robust BOLD fMRI technique with sufficient spatial resolution for functional brain imaging in the mouse has remained technically challenging (Ahrens and Dubowitz, 2001; Huang et al., 1996; Nair and Duong, 2004).

An alternative method for functional MRI in animals uses divalent cationic, manganese ($Mn^{2+}$). $Mn^{2+}$ has two relevant properties: first, its five unpaired electrons make $Mn^{2+}$ a T1-reducing MRI contrast agent; and second, $Mn^{2+}$ can act as a calcium analog, allowing it to enter depolarized neurons cells via voltage-gated calcium channels (Drapeau and Nachshen, 1984; Narita et al., 1990). Taking advantage of these properties, Activation-Induced Manganese-enhanced MRI (AIM MRI) has been used in rats to image neuronal responses to stimuli such as glutamate, cocaine, cerebral ischemia, and electrical paw stimulation (Aoki et al., 2003; Aoki et al., 2002; Duong et al., 2000; Lin and Koretsky, 1997; Lu et al., 2007). Furthermore, this enhancement can be correlated with cerebral blood flow measurements and BOLD contrast (Duong et al., 2000). Because the $Mn^{2+}$ clears slowly from the activated regions, stimulation may be performed outside the magnet prior to imaging providing greater flexibility in experimental design.

One of the challenges with AIM MRI is that $Mn^{2+}$ is excluded by the blood-brain barrier (BBB). In studies to date, $Mn^{2+}$ has been administered acutely to the brain by osmotically opening the BBB with an intracarotid infusion of hypertonic mannitol. To avoid disrupting blood flow to the brain, the mannitol is infused through a catheter placed retrograde to the external carotid artery. While this procedure has been feasible in rats, in mice the technical challenges of osmotic BBB disruption have prevented the use of acute AIM MRI. Instead, a chronic manganese administration paradigm has been adopted for functional brain mapping in mice. In this approach, mice receive a systemic injection of $Mn^{2+}$ and are then exposed to a sustained stimulus for 1–2 days. The manganese diffuses into the brain slowly over several hours and the enhancement pattern seen in post-stimulation MRI reflects an integration of the neuronal activity. This approach is elegant and effective for stimuli amenable to prolonged administration, such as mapping of the auditory cortex (Watanabe et al., 2008; Yu et al., 2005; Yu et al., 2008). However, for more acute stimuli, such as pharmacological challenges or behavioral tasks, a technique would be preferred that uses an immediate administration of $Mn^{2+}$.

To extend the acute AIM MRI to the mouse, a method is needed for rapidly opening the BBB to administer $Mn^{2+}$ to the mouse brain. The most well developed technique is the osmotic technique, mentioned above. However, this has several drawbacks: a) the intra-carotid infusion via the external carotid artery is technically challenging in mice (Zhang et al., 1997); b) the technique is too invasive to use in awake studies or longitudinal studies; and c) the osmotic technique opens the BBB in only a portion of the brain (unilaterally, in the distribution of the internal carotid artery). Recently, focused ultrasound in combination with gas microbubbles (i.e., ultrasound contrast agent) has been used to open the BBB non-invasively and transcranially in mice (Choi et al., 2007a; Choi et al., 2007b; Raymond et al., 2008). To date, this ultrasound technique has only been used to open the BBB in a focal spot.

In this work we use *unfocused* ultrasound and microbubbles to non-invasively open the BBB throughout the *entire* mouse brain (Howles et al., 2008). (For simplicity, the procedure for BBB Opening with Microbubbles and UltraSound is referred to as BOMUS in this paper.) We demonstrate that using BOMUS, $Mn^{2+}$ can be administered throughout the brain parenchyma. We then characterize the temporal dynamics of the $Mn^{2+}$ enhancement from IP and IV administration. Finally, we use this approach to perform AIM MRI in the mouse. This procedure has a number of benefits relative to existing methods: a) immediate administration of $Mn^{2+}$ allows for acute stimulation paradigms; b) the fast and simple

procedure facilitates high-throughput studies; c) the non-invasive technique could permit longitudinal studies and/or stimulation of awake animals; d) opening the whole BBB to $Mn^{2+}$ enables a broader range of stimulation paradigms. We take advantage of these features to map the barrel field cortex response to stimulation of the sinus hairs on the face of the mouse.

The sinus hairs are tactile organs common to most mammals (Woolsey et al., 1975). Sinus hairs (including the vibrissae) on the face of most rodents project on a one-to-one basis to corresponding cytoarchitectural units—known as barrels—in layer IV of the primary sensory cortex. The cortical columns defined by each of these barrels are arranged in roughly the same spatial pattern as the sinus hairs. The large mystacial vibrissae (i.e., the whiskers) are sinus hairs that project to the posterior-medial barrel field. The small vibrissae of the rostral face and lips project to the anterior-lateral barrel field (Welker, 1976). Because the barrel cortex has been extensively mapped in electrophysiology and 2-deoxyglucose studies, it is an excellent system with which to validate activation maps from AIM MRI (McCasland and Woolsey, 1988; Welker, 1976; Welker and Vanderloos, 1986; Woolsey and Van der Loos, 1970; Woolsey et al., 1975).

In this study, AIM MRI in lightly sedated mice was used to map the response in the barrel field to mechanical stimulation of the vibrissae on one side of the face. Because the BOMUS technique opens the BBB throughout the brain, $Mn^{2+}$ was administered to both hemispheres. By comparing the enhancement patterns from stimulated and unstimulated sides of the brain, activation due to the vibrissae stimulation could be distinguished from non-specific background stimulation.

## Materials and Methods

### Microbubbles

Prior to opening the BBB, perflutren lipid microspheres (Definity, Lantheus, N. Billerica, MA) were produced by “activating” the vial (i.e., shaking it in the manufacturer-supplied device for 45 seconds) according to the prescribing information sheet. Immediately prior to microbubble administration, the vial was agitated by hand for 1 minute.

### Ultrasound System

For the ultrasound (Fig. 1), a circular single-element ultrasound transducer (model A382S-SU, Olympus NDT) was used, which had a diameter of 13 mm and a center frequency of 2.15 MHz. The transducer was positioned using a 3-axis frame (VisualSonics, Toronto, ON) at its natural focal distance (58 mm) in a column of water directly over the mouse brain. The transducer was driven by a 50 dB power amplifier (model 240L, E&I, Rochester, NY), which was connected to a signal generator (model 33220A, Agilent, Santa Clara, CA) that produced the ultrasound pulse sequence. The pulse sequence consisted of bursts of 2.15 MHz sinusoidal pulses with 50000 cycles per burst and a burst period of 64 ms. The pulse amplitude was calibrated to generate peak negative acoustic pressures of 0.4 MPa at the center of the transducer’s natural focus. Calibration measurements were made in water using a hydrophone (model SN S4-251, Sonora, Longmont, CO) with a 0.4 mm spot size membrane.

### BBB Opening with Microbubbles and Ultrasound (BOMUS)

All animal studies were approved by the Duke University Institutional Animal Care and Use Committee. A total of 24 C57BL/6 mice were used in this study. For all procedures, mice were anesthetized with isoflurane by nose cone. The respiratory rate was maintained between 85 and 125 breaths-per-minute by titrating the isoflurane concentration. Body

temperature was maintained using a heat lamp (outside the magnet) or blown air (inside the magnet). The nose cone apparatus was designed to fix the animal's head precisely and reliably in the "skull-flat" position (i.e., the dorsal skull surface is horizontal).

Prior to ultrasound, hair was removed from the mouse scalp using an electric trimmer. Ultrasound gel was placed on the scalp, and then a bolus of water contained by a 7.6-μm (0.3 mil) plastic sheet was lowered onto the head (Fig. 1). In this water bolus, the ultrasound transducer was positioned 58 mm directly over the mouse brain. To open the BBB, 30 μL of perflutren lipid microspheres (activated Definity) were injected through a tail vein catheter, and simultaneously, the ultrasound pulse sequence was initiated. The ultrasound was applied for 3 minutes.

### Manganese administration

Manganese chloride ($MnCl_2$-$(H_2O)_4$ Sigma) was prepared at a concentration of 100 mM (300 mOsM) in sterile water. (Note, because the actual molecular weight of hydrated $MnCl_2$ preparations varies considerably, the manufacturer was contacted to determine the molar mass for our particular batch of $MnCl_2$-$(H_2O)_4$, which was 187 g/mol.) In the initial experiment verifying BBB opening, $MnCl_2$ was administered at a dose of 0.4 mmol/kg IV over 60 minutes (beginning 30 min prior to BOMUS). Finally, for AIM MRI, $MnCl_2$ was given at a dose of 0.5 mmol/kg IP, (10 minutes prior to BOMUS).

In preliminary BOMUS studies (using either $MnCl_2$ or Gadolinium-DTPA), IV administration of contrast produced enhancement that was rapid and intense but faded quickly. IP administration produced enhancement that was less intense but more sustained and temporally homogeneous. Therefore, in this work, IP administration was used for AIM MRI because the temporal homogeneity allowed a prolonged stimulation period and made it logistically easier to ensure that all animals were stimulated during the same phase of enhancement. Other experiments (manuscript under review) indicated that the BBB is maximally open at the time of BOMUS and completely closed 4 hours later. Therefore, in this work, $Mn^{2+}$ was given 10 min prior to BOMUS to allow $Mn^{2+}$ to accumulate in the bloodstream so that at the time of BOMUS the $Mn^{2+}$ would be available to enter the brain parenchyma. Stimulation was delayed for 40 minutes to allow $Mn^{2+}$ levels in the brain parenchyma to stabilize. In this way the dramatic baseline enhancement due to $Mn^{2+}$ diffusion across the BBB could be distinguished from the subtle differential enhancement due to the stimulation.

### Vibrissae Stimulation

Vibrissae stimulation was performed on a total of 7 mice: the right side was stimulated in 3 mice, and the left side was stimulated in 4 mice. Prior to $Mn^{2+}$ and BOMUS administration, the vibrissae on the unstimulated side were clipped. This was done under a dissecting microscope with microsurgical scissors to cut the vibrissae as close as possible to the skin surface without irritating the follicle or surrounding skin. After the pre-stimulation imaging (Fig. 2), the isoflurane was turned off and the nose cone was removed. The intact vibrissae were stimulated using a soft artist's paintbrush, which was moved manually in a circular motion (1–5 Hz) through the vibrissae array at a distance of approximately 2–5 mm from the skin. The stimulation was carried out for 90 minutes. For approximately the first 60 minutes of stimulation, the mouse was somewhat somnolent (due to the previous administration of manganese and isoflurane), but still responsive to painful stimuli such as a toe pinch. Because of this somnolence, the mouse tolerated the stimulation well and moved only occasionally. During the latter portion of the stimulation period, the mouse would begin to move more often, and so to sedate the mouse, 5% isoflurane was administered (typically 1–2 times) via nose cone for approximately 15 seconds.

### MR Imaging

For MRI, a 35 mm diameter quadrature transmit/receive volume coil (M2M Imaging, Cleveland, OH) was used. The MR system was a 7 T horizontal bore magnet driven by a GE EXCITE console (GE Healthcare, Milwaukee, WI). MR images were acquired using a 3D spoiled gradient recalled echo (SPGR) sequence with the following parameters: repetition time = 25 ms; echo time = 2 ms; flip angle = 30 degrees; bandwidth = 15.63 kHz; field of view = 20 × 20 × 12 mm; matrix = 128 × 128 × 60.

### Spatial Distribution Analysis

To quantify manganese enhancement of the brain, images were acquired from BOMUS-treated (n = 5) and control (n = 4) mice 170 minutes after IP administration of 0.5 mmol/kg IP $MnCl_2$. BOMUS was performed 10 minutes after $MnCl_2$ administration. Images were registered to a common space by a 12 degree-of-freedom affine registration. Image intensities were normalized using measurements from the extracranial musculature, whose intensity was assumed to be unaffected by opening of the BBB. This normalization made the analysis less sensitive to variations in the MR system or $Mn^{2+}$ dose, but still completely sensitive to variations in BOMUS and $Mn^{2+}$ enhancement of the brain. Then, voxel-wise mean and standard deviation maps were calculated. Finally, for an ROI-based analysis, a segmented reference brain (Johnson et al., 2007) was registered to the same common space, and the mean SNR was measured in each of the following ROIs: cerebral cortex, cerebellum, basal ganglia, brain stem, thalamus, hippocampus, olfactory bulbs, amygdala, hypothalamus, and midbrain.

### AIM MRI Image Analysis

Because the mice were only lightly sedated during stimulation, non-specific background stimulation was expected in all the images. Furthermore, this background stimulation was expected to vary between animals. Therefore, the image analysis sought to identify regions of each brain that had differential signal on the stimulated versus the unstimulated sides of the brain. In addition, the analysis sought to identify which of these differences were statistically significant across animals.

The data analysis scheme is shown in Figure 3. First, the 3D image sets were imported into the Amira software environment (Visage Imaging Inc. Andover, MA). Then, because three of the mice were stimulated on the right and four were stimulated on the left, all brains in which the right vibrissae were stimulated were flipped right-to-left, so that now all the brains were effectively stimulated on the same side. Together, these brains constituted the “left-stimulated” dataset. This combined dataset was then duplicated and flipped right-to-left to create the “left-unstimulated” dataset. All brain images were then registered to a common space by a 12 degree-of-freedom affine registration. Where necessary, preference was give for registering the region of brain between the cerebellum and olfactory bulbs (i.e., the cerebral cortex and underlying structures). The brains were then filtered with 3 × 3 × 3 pixel Gaussian kernel. At this point, the data were transferred to MATLAB (The MathWorks, Natick, MA), and a mask was applied to the brain volumes to select only the brain between the cerebellum and the olfactory bulbs for further analysis. By excluding the extracranial tissues and cerebellum, which did not always register well, the accuracy and computation time of subsequent steps was improved. The masked brains were then intensity-normalized by the iterative method of Venot *et al.* (Cross et al., 2004;Venot et al., 1983). This normalization made the analysis less sensitive to variations in overall manganese enhancement and more sensitive to activation-induced differences in enhancement. A voxel-wise, paired, single-tailed *t* test was used to compare the “left-stimulated” dataset with the “left-unstimulated” dataset. The resultant *p*-value map identified regions where there was consistently elevated signal in one side of the brain relative to the other. Because the test

was *paired*, the voxels in each brain were compared only to the contralateral voxels of the same brain. Because the test was *single tailed*, one side of the *p*-value map showed where the stimulated side had significantly higher signal while the other side of the *p*-value map showed where the unstimulated side had significantly higher signal. In this way, the analysis neither double-counted the brains nor biased the results by assuming the stimulated side would be higher than the unstimulated side. Using this approach, bilateral, non-specific background enhancement could be separated from unilateral, stimulus-specific enhancement; and this stimulus-specific enhancement could be compared across subjects.

## Results

### Administration of Manganese Chloride

The first goal of this work was to demonstrate that $Mn^{2+}$ could be globally administered to the mouse brain by opening the BBB with ultrasound and microbubbles. $Mn^{2+}$ was administered at a dose of 0.4 mmol/kg 30 minutes prior to BOMUS. T1-weighted images were acquired 30 minutes after BOMUS. These images were compared to images from mice that had no treatment or received only $Mn^{2+}$ (i.e., did not receive BOMUS) (Fig. 4). Images from animals (n = 3) not receiving either $Mn^{2+}$ or BOMUS were uniformly dark with no enhancement of any tissues (except the arteries, which had signal from inflowing unsaturated blood). Animals receiving $Mn^{2+}$, but not BOMUS (n = 2), had enhancement of the skin, muscle, and salivary glands. While some enhancement was seen in the choroid plexus and periventricular tissue, the brain parenchyma remained unenhanced because the intact BBB excluded the $Mn^{2+}$. Animals receiving $Mn^{2+}$ and BOMUS (n = 3), showed not only an enhancement of extracranial tissues, but also a dramatic enhancement of the brain parenchyma.

The second step was to assess the spatial distribution of the $Mn^{2+}$ enhancement. $Mn^{2+}$ was administered by IP injection to BOMUS-treated (n = 5) and control animals (n = 4), and T1 weighted images were acquired 170 minutes later. Mean and standard deviation maps were calculated, and SNR measurements were made in 10 different ROIs (Fig. 5). In these results, BOMUS-treated mice had greater enhancement, as more $Mn^{2+}$ entered the brain through the open BBB. However, the mean signal map and ROI measurements show that this enhancement was not uniform, with greater enhancement in the central structures such as the thalamus and hypothalamus. The standard deviation maps showed high variance at the edges of the brain and ventricles. This edge variance was likely due to a combination of true differences in enhancement and registration artifacts.

When these IP $Mn^{2+}$ results are compared to the previous results seen 30 minutes after IV injection of $Mn^{2+}$ (Fig. 4), the difference in signal intensity between BOMUS and control mice appears less dramatic. This smaller difference has two likely reasons: first, in this experiment the $Mn^{2+}$ had more time (170 vs 30 min) to diffuse into the brain in the control mice; and second, with IP administration, less $Mn^{2+}$ is in the blood stream available to enter the brain at the time of BOMUS, when the BBB is maximally opened (Howles et al., 2008).

### Mapping of the Barrel Field Using AIM MRI

Using BOMUS to administer $Mn^{2+}$, AIM MRI was used to map stimulated activity in the barrel cortex. $Mn^{2+}$ was given by IP injection 10 minutes prior to BOMUS, and stimulation was begun 40 minutes after BOMUS. The stimulation was carried out for 90 minutes after which the T1-weighted images were acquired (Fig. 2).

The data analysis compared the stimulated and unstimulated sides of each brain, and it identified differences that were statistically consistent among the animals (Fig. 3). The result was a three-dimensional p-value map (Fig. 8), the right side of which indicated regions of

significantly higher signal *contralateral* to the stimulated vibrissae. The left side of the p-value map indicated which regions had significantly higher signal *ipsilateral* to the stimulated vibrissae. The p-value map—with a threshold of $p < 0.05$—identified a broad region of elevated signal contralateral to the stimulated vibrissae which corresponded to the barrel field of the primary sensory cortex (Figs. 6, 7, 8). Notably, the anterior barrel field had broad coherent activation, while the posterior field had more separate regions pockets of activation.

Because the activation map was a 3D dataset ($156 \times 156 \times 200\ \mu m^3$), the activation regions could be registered to a high-resolution ($21 \times 21 \times 21\ \mu m^3$) 3D brain image (Johnson et al., 2007). By volume-rendering the combined dataset (Fig. 8), the spatial extent of the activation region could be better appreciated and more easily compared to previously published maps of the barrel cortex (Welker, 1976; Woolsey and Van der Loos, 1970). In this way, it was observed that the activated region included not only the posterior-medial barrel field (corresponding to the large mystacial vibrissae) but also the anterior-lateral barrel field (corresponding to the small sinus hairs of the rostral face) (Welker, 1976).

In addition, there were small, scattered points of apparent activation throughout the brain. Because these points were neither coherent nor extensive in size, they likely represent spurious signal. Many of these small points of difference were near the ventricles or the edge of the brain where slight registration errors could lead to spurious differences.

After the study, all 7 mice recovered successfully. When observed 24 hours later, all were active with no apparent signs of distress or locomotor retardation.

## Discussion

In this work, a new method was presented for *non-invasively* administering $Mn^{2+}$ to the *whole mouse brain* using ultrasound and microbubbles. Using this new method, activition-induced manganese-enhanced MRI was used to detect neuronal response to *short-duration* stimulation in *lightly sedated* mice. With this AIM MRI technique, a 3D activation map of the barrel cortex of the mouse was generated.

While manganese-enhanced MRI has been used to map neuronal response to long-term (1–2 days) stimulation in mice (Watanabe et al., 2008; Yu et al., 2005; Yu et al., 2008), this new approach provides a technique for short-term stimulation experiments. Such short-term AIM MRI has been used successfully in rats; however, the need to use mannitol to open the BBB has made it very difficult to extend these studies to mice. Furthermore, even in rats, AIM MRI studies are limited by the interference of non-specific stimuli and the invasiveness of the osmotic BBB disruption. Because the BOMUS technique is non-invasive, it should allow awake stimulation paradigms and longitudinal studies. In this work, the vibrissae stimulation was performed on lightly sedated mice that then recovered fully after the post-stimulation MRI. Furthermore, because BOMUS opens the entire BBB, it also permits a wider range of stimulation paradigms. In this work, the bilateral administration of Mn2+ enabled an analysis that identified the unilateral response to the vibrissae stimulation, while disregarding bilateral activation due to background stimuli.

In this analysis, the *t* test served as useful tool for accounting for variability between animals. Because the analysis made numerous comparisons, when individual voxels or small clusters of voxels are identified as significant by the *t* test, the null hypothesis cannot be rejected using the typical p-value cutoffs. However, because the data are spatially related, when large *contiguous* regions are identified by the *t* test, the null hypothesis can confidently be rejected. The chance of numerous adjacent voxels each being spuriously identified by the *t* test is vanishingly small. Using a threshold of $p < 0.05$, the analysis identified a very large

region that corresponded well to the barrel cortex contralateral to the stimulation. Notably, small changes in the value of *p* value threshold had little effect on the size of the selected region.

The barrel field in mice and rats has been well-characterized electrophysiologically, both in terms of its spatial structure as well as its response to sensory input from the sinus hairs on the face. Being so well characterized, it is an excellent system with which to validate the AIM MRI mapping technique. As seen in Fig. 8, the region of increased neuronal activity identified by AIM MRI corresponded well to published representations of the barrel cortex (Welker, 1976;Woolsey and Van der Loos, 1970).

Notably, both the posterior-medial and anterior-lateral barrel fields responded to the stimulation. While often discussed separately in the literature, these two regions form one continuous barrel field. The posterior-most barrel columns correspond to the long, thick caudal-most vibrissae. Moving rostrally, the vibrissae get progressively shorter and finer while the corresponding barrels, moving anteriorly, also get smaller. While we did our best to stimulate all the vibrissae comparably, the AIM MRI map was more broad and robust in the more anterior parts of the barrel field. This result is consistent with 2-deoxyglucose mapping of the barrel cortex, which has shown greater activation of the barrels corresponding to the more rostral and ventral vibrissae (McCasland and Woolsey, 1988). One explanation for this robust anterior response is that the neuronal density in this region is higher—the anterior field has smaller barrels that are packed at a higher density (Welker, 1976). Furthermore, the anterior field has more cortical volume per peripheral nerve fiber (Welker and Vanderloos, 1986). Because the presumed mechanism for AIM MRI is accumulation of $Mn^{2+}$ in neurons, this higher density and greater number of neurons in the more anterior part of the barrel field may contribute to the more robust AIM MRI enhancement. This explanation is consistent with other workshowing that in non-functional manganese-enhanced MRI, enhancement was greater in regions of high neuronal density (Aoki et al., 2004).

In this study, we stimulated some animals on the left and others on the right rather than stimulating all animals on one side. The reason for stimulating both sides was to demonstrate that any observed AIM MRI effect was due to neuronal activity rather than a systematic error of the experimental setup (such as an asymmetric opening of the BBB). Because the BOMUS procedure was relatively novel, this assurance was deemed worthwhile. However, the drawback of our approach is that because both the left and right animals were analyzed together, this study makes the assumption that both the left and right barrel cortices respond in the same way. While this assumption may not be absolutely true, any left-right differences are likely to be too minor to be reliably detected by the method presented here, even if the left-stimulated and right-stimulated animals were analyzed separately.

It is notable that this activation map was generated in response to mechanical—as opposed to electrical—stimulation of the vibrissae (Fanselow and Nicolelis, 1999). Therefore, the neuronal activation detected was a physiologically realistic response of a mouse to its environment.

This work has demonstrated that by using BOMUS to administer $Mn^{2+}$, AIM MRI can be used in the mouse to identify activated regions. Because the BOMUS technique is noninvasive, these studies can be performed longitudinally. Indeed, all the animals used in this AIM MRI study recovered completely. However, as with all manganese-based techniques, the manganese did have some toxicity (Silva et al., 2004), which in this case was manifest as somnolence during the stimulation period (though they were still responsive to

painful stimuli). Though the precise mechanism for the observed somnolence is not clear, $Mn^{2+}$ is known to have toxic effects on the heart (Jiang and Zheng, 2005), neuromuscular junction (Meiri and Rahamimoff, 1972), and nervous system (Aschner et al., 2007). In this case, the somnolence facilitated the stimulation of the vibrissae, but it may have also suppressed some of the neuronal activity of interest. To minimize this toxicity, further experiments are warranted to determine the minimum effective $Mn^{2+}$ dose for AIM MRI.

In addition to the toxicity of manganese, this technique for AIM MRI has additional limiting factors: uniformity and consistency of the manganese administration; image registration; and unilateral sensitivity. With respect to the manganese administration, the distribution data (Fig. 5) indicate that the BOMUS technique does not provide a homogeneous enhancement of the brain. Thus, regions with a higher baseline enhancement are difficult to distinguish from regions whose elevated signal is due to neuronal activity. We obviated this limitation in this study by using the contralateral side of the brain as an internal control, however this option would not be available in a bilateral study. Though not uniform across the brain, the pattern of baseline enhancement was fairly consistent across individuals. However, the degree of this consistency is a fundamental limitation on the sensitivity of the technique. Minor variations in this baseline enhancement (possibly due to variations in the BBB opening) can potentially mask the AIM MRI signal. To account for this variation, we averaged the effect over several animals. An alternative solution may have been to repeat the experiment several times on the same animal or to acquire pre-stimulation baseline images.

Because of this need for statistical analysis of multiple brains, image registration is critical. For example, the high variance seen in enhancement seen at the edges of the brain and ventricles (Fig. 5) were likely due largely to registration artifacts. Thus, regions that are susceptible to registration errors are difficult to study (e.g., the cerebellum and olfactory bulbs, which are layered and often not aligned with the rostral-caudal axis). In this work, the cerebellum and olfactory bulbs were excluded *a priori*, but the use of nonlinear registration techniques may allow their study in future experiments. Indeed, image registration may be the limiting factor in the spatial resolution of this technique—a slight misregistration could average-out very small regions of enhancement. Despite this difficulty, future experiments are needed to evaluate the spatial resolution of this method of AIM MRI. For example, by stimulating only a subset of vibrissae, the smallest detectable region of cortex could be determined.

This study looked for differences between the two sides of the brain in order to identify the unilateral effects of vibrissae stimulation. This allowed the study to be robust to variability of manganese administration and to minimize background stimulation artifacts. However, the study was therefore inherently insensitive to bilateral effects. A study that sought to detect bilateral effects would likely need separate control animals. Because each animal would no longer act as its own control, variations in the background stimulation (e.g., the sensory experience in the laboratory) would interfere with detection of the response to the vibrissae stimulation. Though this could be overcome by averaging data from more mice, the total number of animals would increase significantly.

Future experiments are needed to determine the spatial and temporal resolution of this method of AIM MRI. For example, by stimulating only a subset of vibrissae, the smallest detectable region of cortex could be determined. However, the analysis over several animals would require extremely precise image registration—a slight misregistration could average-out very small regions of enhancement. The temporal resolution of this technique is also unclear. While the 90-minute stimulation regimen used in this work was considerably shorter than the 1–2 days used in other MEMRI cortical mapping studies in mice (Watanabe et al., 2008; Yu et al., 2005; Yu et al., 2008), it may have still been much longer than

needed. While experiments could be designed to determine the minimum duration of stimulation, a more exciting possibility would be to use BOMUS to perform dynamic AIM MRI (Aoki et al., 2002), in which the stimulus is administered in the magnet while serial scans are acquired. If successful, such an approach would bring many of the benefits of human fMRI to the study of mouse models.

## Conclusions

Manganese can be administered to the whole brain of the mouse using transcranial ultrasound with microbubbles to open the blood-brain barrier. Because the procedure is simple, fast, and non-invasive, it is suitable for high-throughput and longitudinal studies. By administering manganese in this way, activation-induced manganese-enhanced MRI can potentially be performed in awake mice. In this work, such an approach was used on lightly sedated mice to create a 3D map of the barrel field corresponding to the mystacial and rostral vibrissae was created which agreed well with the existing literature. Because the ultrasound opened the blood-brain barrier throughout the brain, the unstimulated side of the brain could be used to control for non-specific background stimulation. This use of ultrasound to administer manganese enables a new method for functional neuroimaging in the mouse.

## Acknowledgments

We wish to thank several colleagues: Anastasiya Batrachenko for assistance in data acquisition; Shella Keilholz for valuable discussions regarding the execution and analysis of the experiment; Waqas Majeed for sharing his MATLAB code, which served as a template for our data analysis; Romulo Fuentes and Eric Thomson for valuable discussions regarding vibrissae stimulation; and Sally Zimney for assistance with manuscript preparation. All work was performed at the Duke Center for In Vivo Microscopy, an NIH/NCRR national Biomedical Technology Research Center (P41 RR005959) and NCI Small Animal Imaging Resource Program (U24 092656).

## References

Ahrens ET, Dubowitz DJ. Peripheral somatosensory fMRI in mouse at 11.7 T. NMR in Biomedicine 2001;14:318–324. [PubMed: 11477652]

Aoki I, Ebisu T, Tanaka C, Katsuta K, Fujikawa A, Umeda M, Fukunaga M, Takegami T, Shapiro EM, Naruse S. Detection of the anoxic depolarization of focal ischemia using manganese-enhanced MRI. Magnetic Resonance in Medicine 2003;50:7–12. [PubMed: 12815672]

Aoki I, Tanaka C, Takegami T, Ebisu T, Umeda M, Fukunaga M, Fukuda K, Silva AC, Koretsky AP, Naruse S. Dynamic activity-induced manganese-dependent contrast magnetic resonance imaging (DAIM MRI). Magnetic Resonance in Medicine 2002;48:927–933. [PubMed: 12465100]

Aoki I, Wu YJL, Silva AC, Lynch RM, Koretsky AP. In vivo detection of neuroarchitecture in the rodent brain using manganese-enhanced MRI. Neuroimage 2004;22:1046–1059. [PubMed: 15219577]

Aschner M, Guilarte TR, Schneider JS, Zheng W. Manganese: Recent advances in understanding its transport and neurotoxicity. Toxicology and Applied Pharmacology 2007;221:131–147. [PubMed: 17466353]

Choi JJ, Pernot M, Brown TR, Small SA, Konofagou EE. Spatio-temporal analysis of molecular delivery through the blood-brain barrier using focused ultrasound. Physics in Medicine and Biology 2007a;52:5509–5530. [PubMed: 17804879]

Choi JJ, Pernot M, Small SA, Konofagou EE. Noninvasive, transcranial and localized opening of the blood-brain barrier using focused ultrasound in mice. Ultrasound in Medicine and Biology 2007b; 33:95–104. [PubMed: 17189051]

Cross DJ, Minoshima S, Anzai Y, Flexman JA, Keogh BP, Kim YM, Maravilla KR. Statistical mapping of functional olfactory connections of the rat brain in vivo. Neuroimage 2004;23:1326–1335. [PubMed: 15589097]

Drapeau P, Nachshen DA. Manganese fluxes and manganese-dependent neurotransmitter release in presynaptic nerve-endings isolated from rat-brain. Journal of Physiology-London 1984;348:493–510.

Duong TQ, Silva AC, Lee SP, Kim SG. Functional MRI of calcium-dependent synaptic activity: Cross correlation with CBF and BOLD measurements. Magnetic Resonance in Medicine 2000;43:383–392. [PubMed: 10725881]

Fanselow EE, Nicolelis MAL. Behavioral modulation of tactile responses in the rat somatosensory system. Journal of Neuroscience 1999;19:7603–7616. [PubMed: 10460266]

Howles, G.; Frinkley, K.; Qi, Y.; Nightingale, K.; Johnson, G. Opening the blood brain barrier with ultrasound for in vivo contrast-enhanced imaging of the mouse brain. Proceedings 16th Scientific Meeting, International Society for Magnetic Resonance in Medicine; Toronto. 2008. p. 2306

Huang W, Palyka I, Li HF, Eisenstein EM, Volkow ND, Springer CS. Magnetic resonance imaging (MRI) detection of the murine brain response to light: Temporal differentiation and negative functional MRI changes. Proceedings of the National Academy of Sciences of the United States of America 1996;93:6037–6042. [PubMed: 8650215]

Jiang YM, Zheng W. Cardiovascular toxicities upon manganese exposure. Cardiovascular Toxicology 2005;5:345–354. [PubMed: 16382172]

Johnson GA, Ali-Sharief A, Badea A, Brandenburg J, Cofer G, Fubara B, Gewalt S, Hedlund LW, Upchurch L. High-throughput morphologic phenotyping of the mouse brain with magnetic resonance histology. Neuroimage 2007;37:82–89. [PubMed: 17574443]

Lin YJ, Koretsky AP. Manganese ion enhances T-1-weighted MRI during brain activation: An approach to direct imaging of brain function. Magnetic Resonance in Medicine 1997;38:378–388. [PubMed: 9339438]

Lu HB, Xi ZX, Gitajn L, Rea W, Yang YH, Stein EA. Cocaine-induced brain activation detected by dynamic manganese-enhanced magnetic resonance imaging (MEMRI). Proceedings of the National Academy of Sciences of the United States of America 2007;104:2489–2494. [PubMed: 17287361]

McCasland JS, Woolsey TA. High-Resolution 2-Deoxyglucose Mapping of Functional Cortical Columns in Mouse Barrel Cortex. Journal of Comparative Neurology 1988;278:555–569. [PubMed: 3230170]

Meiri U, Rahamimoff R. Neuromuscular transmission - inhibition by manganese ions. Science 1972;176:308. [PubMed: 5019787]

Nair G, Duong TQ. Echo-planar BOLD fMRI of mice on a narrow-bore 9.4 T magnet. Magnetic Resonance in Medicine 2004;52:430–434. [PubMed: 15282829]

Narita K, Kawasaki F, Kita H. Mn and Mg Influxes through Ca channels of motor-nerve terminals are prevented by verapamil in frogs. Brain Research 1990;510:289–295. [PubMed: 2158851]

Paxinos, G.; Franklin, KBJ. The Mouse Brain in Stereotaxic Coordinates. 2. Academic Press; San Diego: 2001.

Raymond SB, Treat LH, Dewey JD, McDannold NJ, Hynynen K, Bacskai BJ. Ultrasound enhanced delivery of molecular imaging and therapeutic agents in Alzheimer's disease mouse models. PLoS ONE 2008;3:e2175. [PubMed: 18478109]

Silva AC, Lee JH, Aoki L, Koretsky AR. Manganese-enhanced magnetic resonance imaging (MEMRI): methodological and practical considerations. Nmr in Biomedicine 2004;17:532–543. [PubMed: 15617052]

Venot A, Lebruchec JF, Golmard JL, Roucayrol JC. An automated-method for the normalization of scintigraphic images. Journal of Nuclear Medicine 1983;24:529–531. [PubMed: 6854401]

Watanabe T, Frahm J, Michaelis T. Manganese-enhanced MRI of the mouse auditory pathway. Magnetic Resonance in Medicine 2008;60:210–212. [PubMed: 18581385]

Welker C. Receptive-fields of barrels in somatosensory neocortex of rat. Journal of Comparative Neurology 1976;166:173–189. [PubMed: 770516]

Welker E, Vanderloos H. Quantitative correlation between barrel-field size and the sensory innervation of the whiskerpad - a comparative-study in 6 strains of mice bred for different patterns of mystacial vibrissae. Journal of Neuroscience 1986;6:3355–3373. [PubMed: 3772437]

Woolsey TA, Van der Loos H. Structural organization of layer-iv in somatosensory region (si) of mouse cerebral cortex. description of a cortical field composed of discrete cytoarchitectonic units. Brain Research 1970;17:205–242. [PubMed: 4904874]

Woolsey TA, Welker C, Schwartz RH. Comparative anatomical studies of sml face cortex with special reference to occurrence of barrels in layer-4. Journal of Comparative Neurology 1975;164:79–94. [PubMed: 809494]

Yu X, Wadghiri YZ, Sanes DH, Turnbull DH. In vivo auditory brain mapping in mice with Mn-enhanced MRI. Nature Neuroscience 2005;8:961–968.

Yu X, Zou J, Babb JS, Johnson G, Sanes DH, Turnbull DH. Statistical mapping of sound-evoked activity in the mouse auditory midbrain using Mn-enhanced MRI. Neuroimage 2008;39:223–230. [PubMed: 17919926]

Zhang ZG, Chopp M, Zhang RL, Goussev A. A mouse model of embolic focal cerebral ischemia. Journal of Cerebral Blood Flow and Metabolism 1997;17:1081–1088. [PubMed: 9346433]

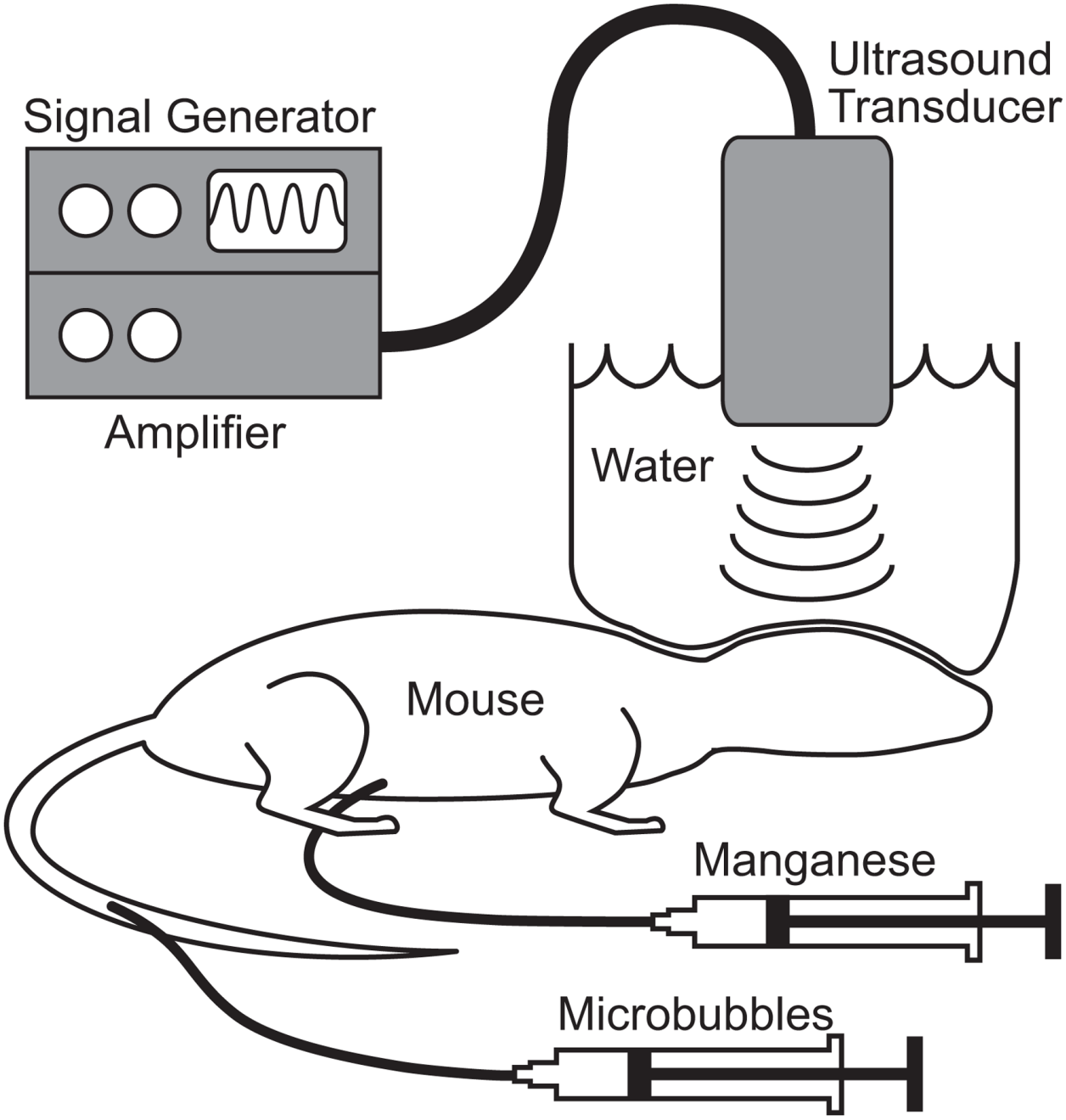


**Figure 1.**
Setup for Blood-brain barrier Opening with Microbubbles and UltraSound (BOMUS): manganese is injected 10 minutes prior to the study, then the BBB is opened by injecting microbubbles and simultaneously insonating the brain for 3 minutes.

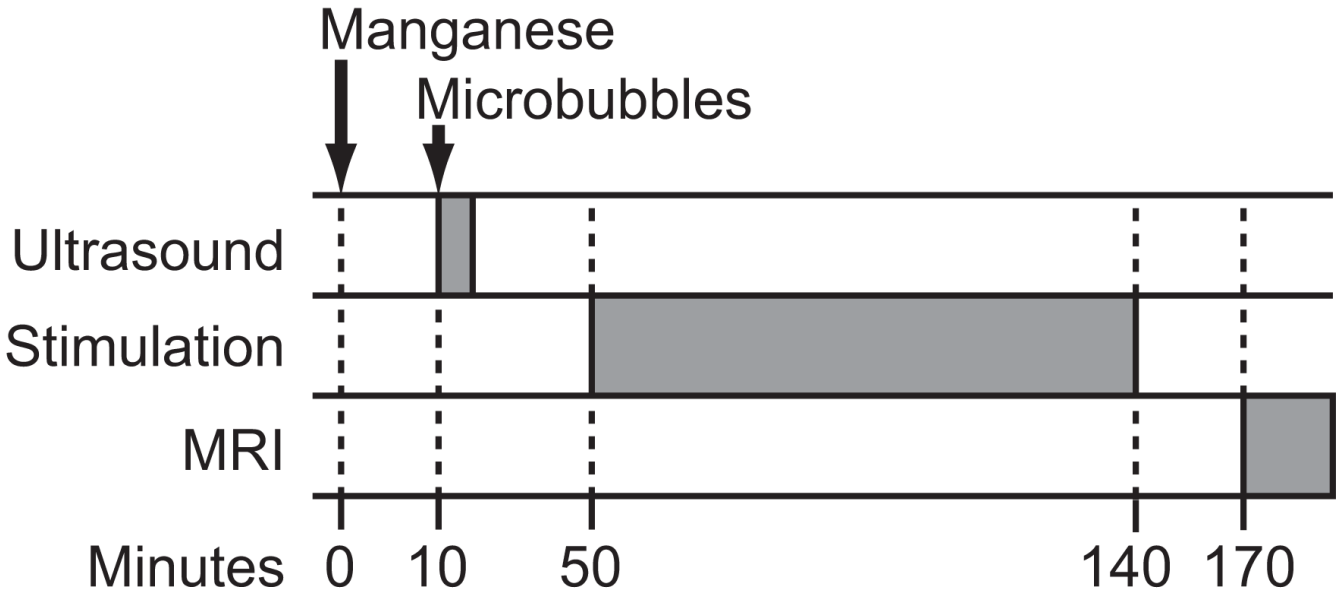


**Figure 2.**
Timeline for activation-induced manganese-enhanced MRI experiment.

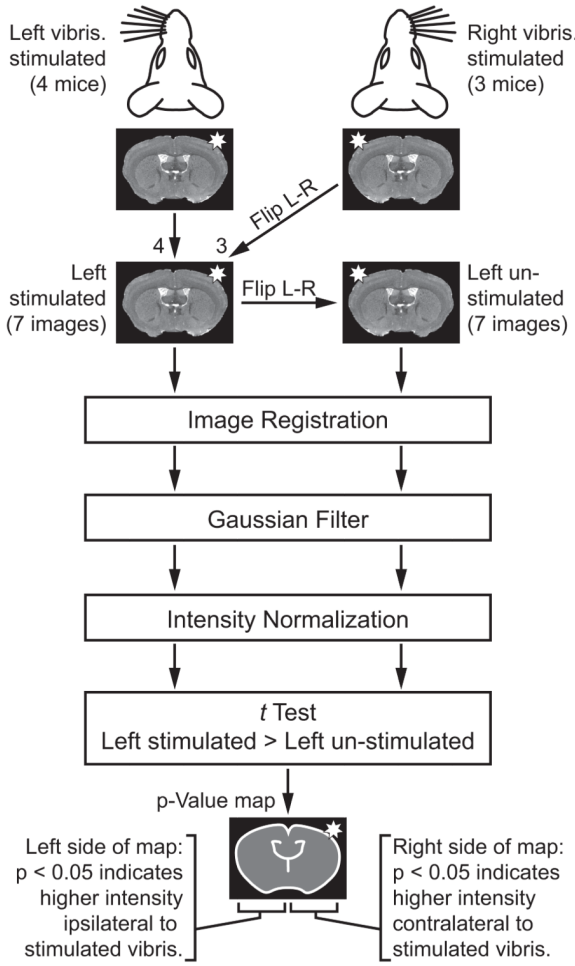


**Figure 3.**

Analysis scheme for identifying regions of different intensity between the stimulated and unstimulated sides of each brain. First all *right-stimulated* images were flipped R-L so that all brains (7 images) were effectively *left-stimulated*. Then, to compare the stimulated side of each image to the unstimulated side, a duplicated but mirrored *left-unstimulated* image set was created. All these images were registered, filtered, and normalized. Finally a *t* test compared the *left-stimulated* and *left-unstimulated* images. The *t* test was "paired" so that the stimulated side of each brain was only compared to the unstimulated side of the *same* brain. The *t* test was "single-tailed" so that one side of the *p*-value map would indicate significantly higher signal on the *stimulated* side of the brain, while the other side of the *p*-value map would indicate significantly higher signal on *unstimulated* side of the brain.

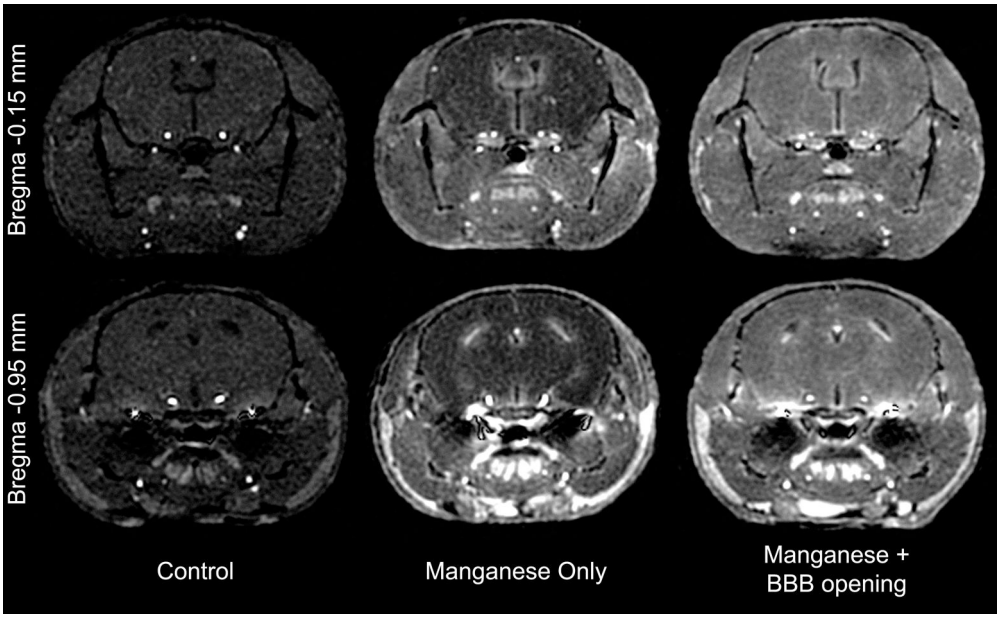


**Figure 4.**
T1-weighted images demonstrating the distribution of manganese with and without BOMUS. Two axial slices are shown, one from a rostral position (top row) and one from a caudal position (bottom row). Animals receiving only Mn2+ had enhancement of the extracranial tissues (skin, muscle, glands), but the intact BBB excluded Mn2+ from the brain parenchyma. However, in mice receiving BOMUS, Mn2+ crossed the BBB and enhanced the brain parenchyma.

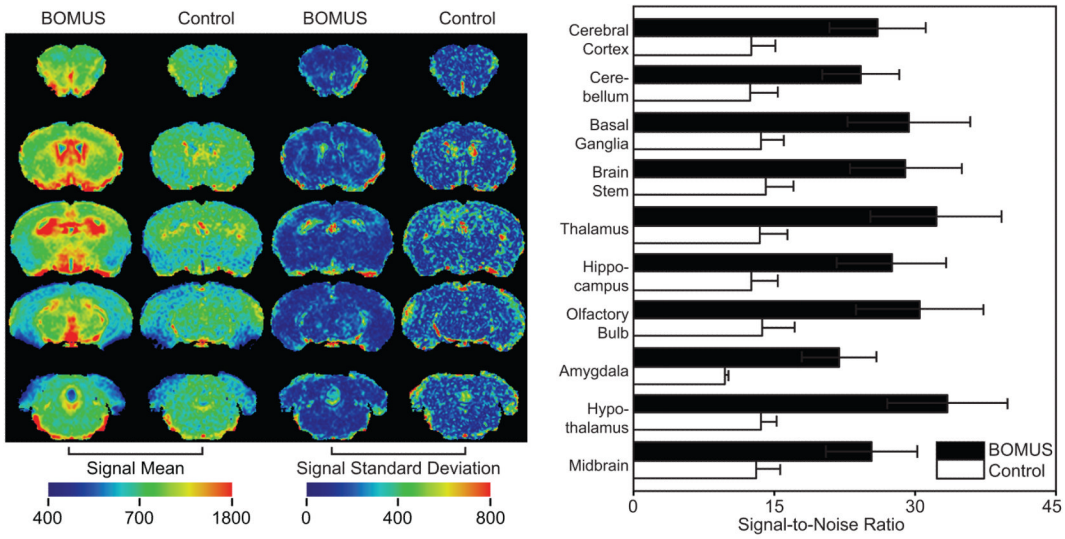


**Figure 5.**

Spatial distribution of $Mn^{2+}$ in the brain. Images were acquired 170 minutes after 0.5 mmol/kg IP $MnCl_2$ from BOMUS-treated (n = 5) and control (n = 4) mice. After normalization, mean and standard deviation maps were calculated (left panel). Enhancement was greater in the BOMUS-treated mice. Though this enhancement was not uniform across the brain, it was fairly consistent, except near the edges of the brain and ventricles. Using ROIs drawn around various structures, the mean SNR (+1 SD) was calculated across each group (right panel). BOMUS-treated animals showed greater SNR but also greater variance between structures and between animals.

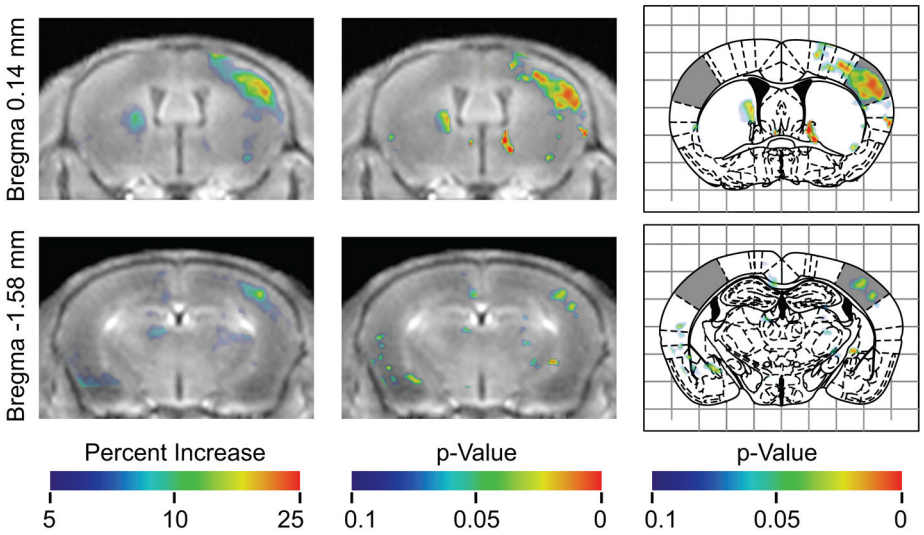


**Figure 6.**

Results of pooled analysis of 7 animals at two different axial positions. The first column shows the mean of all registered images aligned, so that effectively all mice had their left vibrissae stimulated. These images are overlaid with a color map indicating the average percent *increase* in signal at each voxel relative to the *contralateral* side, as indicated by the color bar. Colored regions on the right side of the image show where the side *contralateral* to the stimulation had higher signal. Colored regions on the left side of the image show where the side *ipsilateral* to the stimulation had higher signal. The second column shows the same images overlaid with the p-value map indicating the statistical significance of the increase in signal. The third column shows the same p-value map overlaid on the corresponding figures from the Paxinos stereotaxic atlas (Paxinos and Franklin, 2001) with the barrel fields of the sensory cortex shaded.

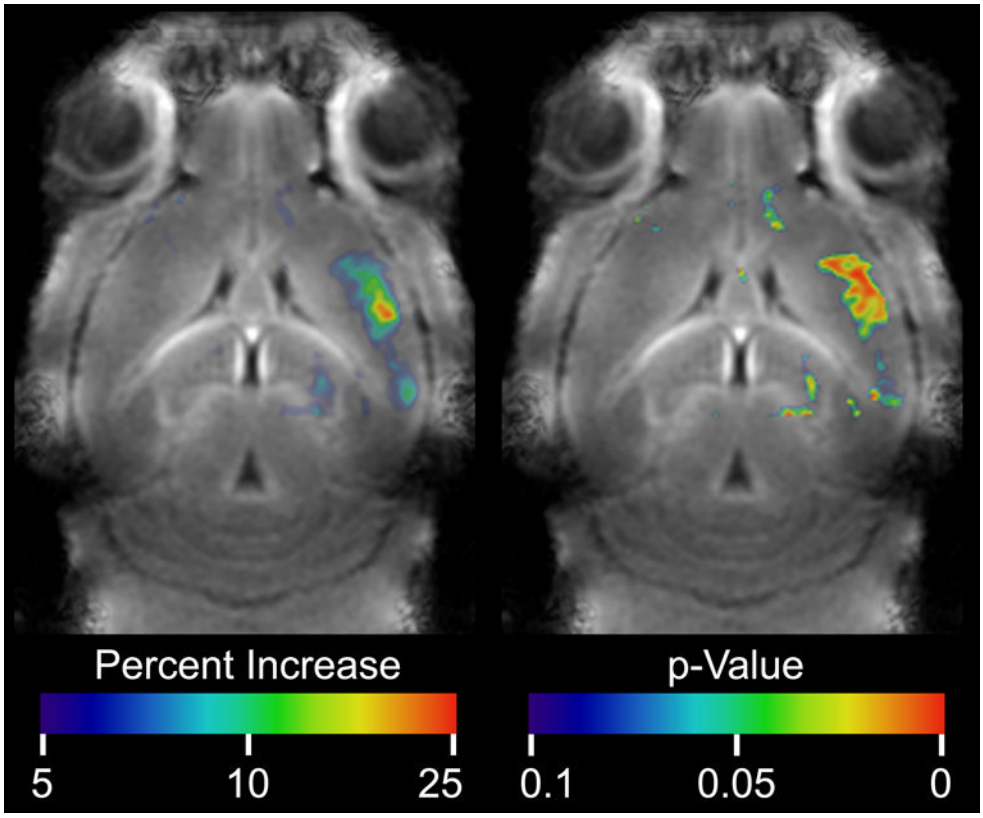


**Figure 7.**
Coronal images show the mean of all registered images aligned, so that effectively all mice had their left vibrissae stimulated. On the left, the image is overlaid with a color map indicating the average percent *increase* in signal at each voxel relative to the *contralateral* side, as indicated by the color bar. Colored regions on the right side of the image show where the brain *contralateral* to the stimulation had higher signal. Colored regions on the left side of the image show where the brain *ipsilateral* to the stimulation had higher signal. The second column shows the same images overlaid with the p-value map indicating the statistical significance of the increase in signal.

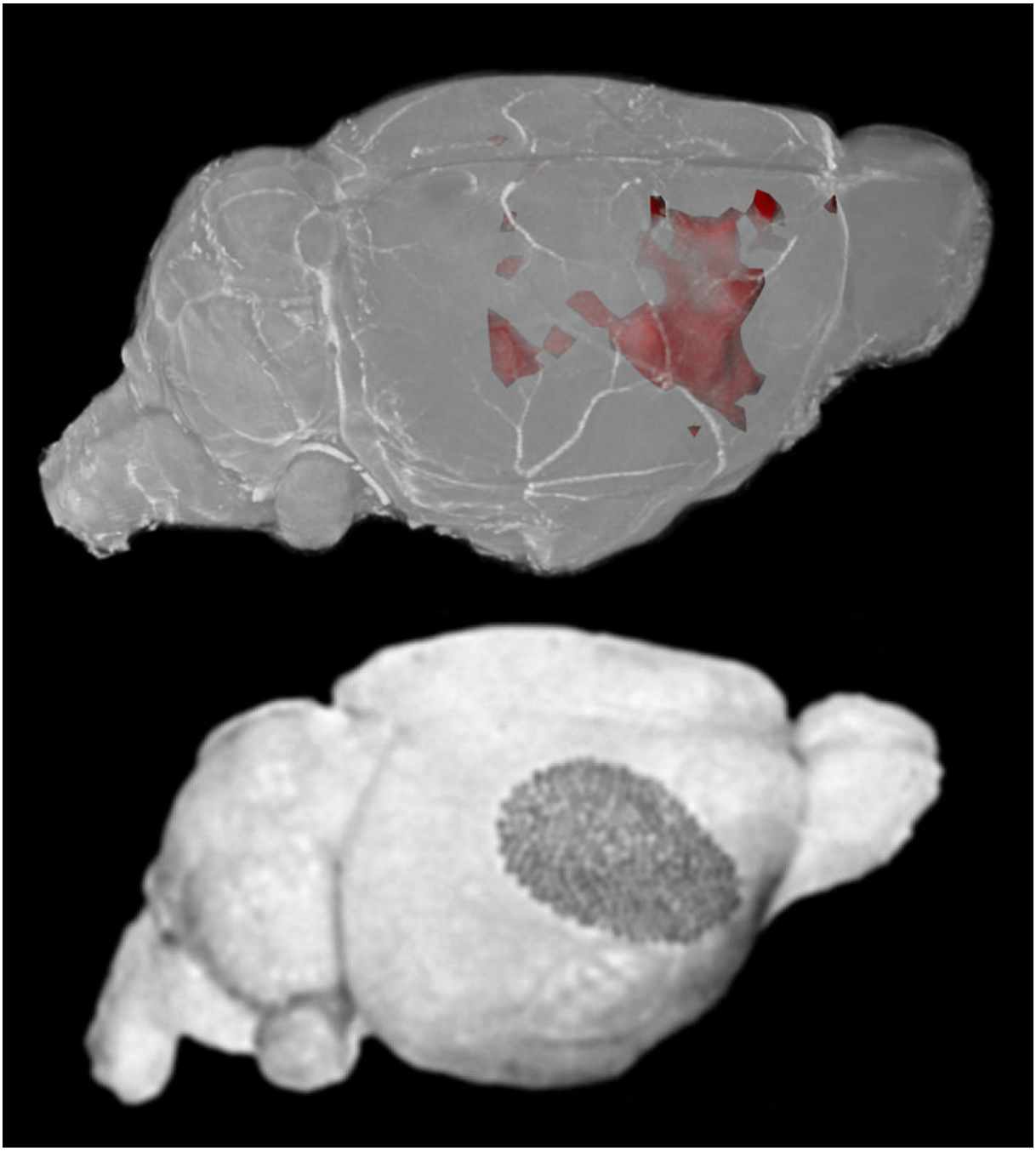

**Figure 8.**

The upper image shows a volume rendering of a high-resolution mouse brain dataset. The p-value map, thresholded at $p < 0.05$, is surface rendered in red. The lower image shows is reproduced from (Woolsey and Van der Loos, 1970) showing the cytoarchitecturally defined map of the mouse barrel cortex. Excellent agreement is seen between the two maps, though less activation is seen in the posterior medial barrel cortex.